Title

Assembling and Redispersibility of Rice Straw Nanocellulose: Effect of tert-Butanol

Journal

ACS Applied Materials & Interfaces, 6(22)

ISSN

1944-8244

Authors

Jiang, Feng

Hsieh, You-Lo

Publication Date

2014-11-26

DOI

10.1021/am505626a

Peer reviewed

ACS APPLIED MATERIALS & INTERFACES

Research Article

www.acsami.org

Assembling and Redispersibility of Rice Straw Nanocellulose: Effect of *tert*-Butanol

Feng Jiang and You-Lo Hsieh*

Fiber and Polymer Science, University of California, Davis, California 95616, United States

Supporting Information

ABSTRACT: Self-assembling of sulfuric-acid-hydrolyzed cellulose nanocrystals (CNCs, 6.4 nm wide) and TEMPO oxidized cellulose nanofibrils (CNFs, 2.1 nm wide) from aqueous suspensions was induced by rapid freezing (−196 °C, 10 min) and slow lyophilization (−50 °C, 0.05 mbar, 2 days). The assembled structures contain submicron (200−700 nm) wide and tens of micrometer long fibers at up to 0.1−0.5% and 0.01−0.05%, the critical fiber-to-film transformation concentrations for CNCs and CNFs, respectively. The assembled fiber widths were significantly reduced to ∼40 nm, that is, by 1 order of magnitude, when 10% of the aqueous media was replaced with *tert*-butanol. Further increasing *tert*-butanol contents in the media to 93/7 (CNCs) and 50/50 (CNFs) *tert*-butanol/water, both at 0.1% nanocellulose concentration, reduced longitudinal assembling for CNCs and lateral assembling for CNFs as well as increased critical fiber-to-film transformation concentration for CNFs. While all assembled structure could be redispersed in water, those from *tert*-butanol/water could also be easily redispersed in DMF aided with brief 2 min ultrasonication. None of the assembled structures could be redispersed in the lower dielectric constant ethanol, acetone or chloroform.

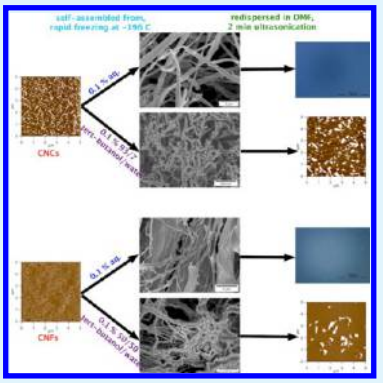

KEYWORDS: *cellulose nanocrystals, cellulose nanofibrils, self-assembly, redispersibility, rice straw*

1. INTRODUCTION

Native cellulose is in hierarchical fibrillar structure consisting of microfibrils,[1,2] which could be isolated by biochemical, chemical, and mechanical means into nanocellulose that are ∼3−20 nm wide, 100 nm to several micrometers long and varied degree of crystallinity.[3−6] The unique nanoscale lateral dimensions,[7,8] high aspect ratio,[8] high specific surface,[9] superior elastic modulus (150 GPa),[10] and tensile strength (2−6 GPa),[11] along with low thermal expansion coefficient (10^{-7} K^{-1})[12] of these nanocellulose have stimulated tremendous interests in research

To date, both cellulose nanocrystals (CNCs) from sulfuric acid hydrolysis[2,13−17] and nanofibrils (CNFs) from 2,2,6,6-tetramethylpiperidine (TEMPO) oxidation[5,18−21] represent two of the most reported nanocellulose, with the latter being often coupled with mechanical forces to improve defibrillation efficiency and dimensional uniformity. The respective surface anionic sulfate and carboxylic groups on these nanocellulose surfaces also help to stabilize their aqueous suspensions. Irrespective of defibrillation approaches, the various forms of nanocellulose derived are typically in dilute aqueous suspensions whose excessive water can be removed or driven off by drying in processes, such as ultrafiltration,[22,23] freeze-drying,[24−26] supercritical drying,[27−29] spray drying,[28] and air drying.[9] Among them, freezing followed by freeze-drying is the most common, but causes nanocellulose to agglomerate into various bulk morphologies of fibers, ribbons and films, etc.,[7,8,24,25] losing the desirable nanoscale characteristics.

Some of the morphologies have been associated with nanocellulose characteristics, freezing and media conditions. For instance, freezing uncharged CNFs derived from different methods (enzymatic hydrolysis,[30] ultrasonication,[31,32] blending[7]) and sources (bamboo,[31] wheat straw,[31] rice straw,[7] and softwood[30−32]) as aqueous suspensions at various concentrations (0.05%,[7,31] 0.2[32]−2%[30]) and temperatures (−20,[31,32] −180,[30] or −196 °C[7]), followed by freeze-drying led to 30 nm[30] to up to 100[31] and 150[7,32] nm wide fibers. Freezing (196 °C) and freeze-drying of negatively charged sulfuric acid hydrolyzed CNCs also produced fibers,[7,8,33−35] but also nanoparticle clusters and micrometer wide ribbons in some cases.[33,34] More highly charged CNCs assembled into much thinner and more uniform submicron fibers,[7,35] but TEMPO oxidized CNFs with more total carboxylic (COOH) and carboxylate (COO^-Na^+) groups formed wider fibrillar structures.[8] In addition, freezing temperature[27] and dispersing medium[9,15] have also shown to influence the dried morphologies. Freezing 0.6% TEMPO oxidized CNFs at −20 and −196 °C has shown to generate different pore and assembled solid morphologies, attributing to the distinct ice crystal growth from different freezing rates.[36] Exchanging water in CNF suspensions with *tert*-butanol reduced the fiber widths to as small as 10−40 nm.[9,24] However, both works exchanged water completely to *tert*-butanol in laborious steps and the

Received: August 22, 2014
Accepted: October 20, 2014
Published: October 23, 2014

effects of nanocellulose characteristics and freezing environments have not been clearly elucidated to draw clear relationship to the assembled morphologies.

In this study, freezing induced self-assembled morphologies of rice straw nanocellulose was systematically investigated by varying the major parameters of nanocellulose characteristics, media compositions, and freezing conditions. Sulfuric acid hydrolyzed CNCs and TEMPO oxidized CNFs that differ in sizes, aspect ratios as well as surface charge species and extent were used and the effects of nanocellulose concentrations, freezing temperatures, and *tert*-butanol as codispersing media on the assembled morphologies to limit hydrogen bonding among nanocellulose were investigated. In addition, redispersibility of the assembled CNC and CNF solids in aqueous and organic solvents with minimal sonication was observed to give further insight into the nature of the assembled interfaces and the potential to expand processing and applications. Lyophilized CNCs have shown to be dispersible into organic solvents, that is, dimethyl sulfoxide, *N*,*N*,-dimethylformamide, formic acid, *m*-cresol, *N*-methyl pyrrolidone, following prolonged sonication (6−72 h).[37−43] Redispersibility of lyophilized CNFs has not been reported, except for solvent exchanging never-dried TEMPO oxidized CNFs into polar solvents.[44]

2. EXPERIMENTAL SECTION

2.1. Materials. Pure cellulose was isolated from rice straw to 36% yield by a three-step 2:1 toluene/ethanol extracting, acidified $NaClO_2$ (1.4%, pH 3−4, 70 °C, 6 h) and KOH (5%, 90 °C, 2 h) isolation process reported previously.[33] Sulfuric acid (H_2SO_4, 95−98%, ACS GR, EMD), hydrochloric acid (HCl, 1 N, Certified, Fisher Scientific), sodium hydroxide (NaOH, 1 N, Certified, Fisher Scientific), sodium hypochlorite (NaClO, 11.9%, reagent grade, Sigma-Aldrich), 2,2,6,6-tetramethylpiperidine (TEMPO, 99.9%, Sigma-Aldrich), sodium bromide (NaBr, BioXtra, 99.6%, Sigma-Aldrich), *tert*-butanol (Certified, Fisher Scientific), acetone (histological grade, Fisher Scientific), ethanol (anhydrous, histological grade, Fisher Scientific), *N*,*N*-dimethylformamide (DMF, HPLC grade, EMD), and chloroform (HPLC grade, EMD) were used as received. CNCs were isolated using 64% sulfuric acid at 45 °C for 45 min with acid-to-cellulose ratio of 8.75 mL/g.[7] CNFs were defibrillated via TEMPO oxidation employing 5 mmol/g NaClO/cellulose at pH 10, with pH adjusting to 7 at end of oxidation to partially convert carboxylate (COO^-Na^+) to carboxylic (COOH), followed by mechanical blending (Vitamix 5200) at 37 000 rpm for 30 min.[8] All water used was purified by Milli-Q plus water purification system (Millipore Corporate, Billerica, MA). Weight/volume percent (%) was used to denote the concentrations of all nanocellulose suspensions.

2.2. Characterization of Individual CNCs and CNFs. Both CNCs and CNFs (10 μL, 0.002%) were deposited onto a freshly cleaved mica surface, air-dried and scanned by an Asylum-Research MFP-3D atomic force microscope using tapping mode with OMCL-AC160TS standard silicon probes, with the average thickness being determined from the height profiles of ca. 200 representative particles with MFP3D 090909 + 1409 plugin in IGOR Pro 6.21. CNC and CNF suspension (8 μL, 0.01%) was deposited onto glow-discharged carbon-coated TEM grids (300-mesh copper, Formvar-carbon, Ted Pella Inc., Redding, CA) and the excess liquid was removed by blotting with a filter paper after 10 min, followed by negatively staining with 2% uranyl acetate for 5 min, and dried under ambient condition. The samples were observed using a Philip CM12 transmission electron microscope operated at a 100 kV accelerating voltage. The average width and length were determined from TEM images of over 200 samples using analySIS FIVE software. The surface sulfate (OSO_3H), carboxylic (COOH) and carboxylate (COO^-Na^+) contents were determined from conductometric titration using OAKTON pH/Con 510 series meter, as detailed described previously (detailed method is provided in Supporting Information).[8] The surface charge density was normalized by cellulose mass or anhydroglucose (AG) unit.

2.3. Self-Assembly of CNCs and CNFs by Freeze-Drying. Self-assembling of CNCs and CNFs was observed under varied media compositions and conditions as summarized in Table 1. Aqueous

Table 1. Freezing Conditions for CNC and CNF Self-Assembly

samples	dispersion media	concentrations (%)	freezing temperature (°C)
CNCs	water	0.001−1	−196
	water	0.05	−20
	10/90 *tert*-butanol/water	0.05−0.5	−196
	93/7 *tert*-butanol/water	0.1	−196
CNFs	water	0.01−0.3	−196
	water	0.01	−20
	10/90 *tert*-butanol/water	0.01−0.1	−196
	50/50 *tert*-butanol/water	0.1	−196

CNC (0.001−1%) and CNF (0.01−0.3%) suspensions (20 mL) in 50 mL centrifuge tubes were quickly frozen by immersing in liquid nitrogen (−196 °C) for 10 min then lyophilized (−50 °C, 0.05 mbar) for 2 days in a freeze-drier (FreeZone 1.0L Benchtop Freeze-Dry System, Labconco, Kansas City, MO). To compare freezing temperature effect, CNC (0.05%) and CNF (0.01%) aqueous suspensions were frozen at −20 °C for 6 h and then lyophilized as previously described. To study the effect of dispersing media, 10 vol % of *tert*-butanol was added into CNC and CNF suspensions, and sonicated for 5 min (Branson ultrasonic processor model 2510, Danbury, CT), making CNCs and CNFs 10/90 *tert*-butanol/water suspension at 0.05−0.5% and 0.01−0.1%, respectively. To investigate the effect of *tert*-butanol concentration, higher *tert*-butanol/water ratios of 93/7 and 50/50 were used for CNC and CNF, respectively, making final 0.1% nanocellulose concentration. The *tert*-butanol/water suspensions were frozen using liquid nitrogen and freeze-dried as previously described.

2.4. Characterization of Self-Assembled CNCs and CNFs. The freeze-dried samples were imaged by a field emission scanning electron microscope (FE-SEM) (XL 30-SFEG, FEI/Philips, USA) at a 5 mm working distance and 5 kV accelerating voltage. The samples were mounted on substrates with fixed conductive carbon tape and then sputter coated with gold for 2 min. The diameters of assembled fibers were calculated from measurements of over 100 individual fibers using an image analyzer (ImageJ, NIH, USA).

The Brunauer−Emmett−Teller (BET) specific surface areas of assembled CNCs and CNFs from 0.1% aqueous and *tert*-butanol/water suspension were determined by N_2 adsorption at 77 K with a surface area and porosity analyzer (ASAP 2000, Micromeritics, USA). Before measurement, the samples were first degassed at 35 °C for 24 h. The specific surface areas were determined by the BET method from the adsorption and desorption isotherms.[45] Pore size distributions were derived from desorption branch of the isotherms by the Barrett−Joyner−Halenda (BJH) method.[46] The total pore volumes were estimated from the amount adsorbed at a relative pressure of $P/P_0 = 0.98$.

2.5. Redispersibility of Self-Assembled CNCs and CNFs. CNCs and CNFs freeze-dried from 0.1% aqueous and *tert*-butanol/water (93/7 and 50/50 for CNCs and CNFs, respectively) suspensions were redispersed in various solvents by brief 2 min ultrasonication (Misonix ultrasonic liquid processors S4000). Weighted amounts (10 mg) of freeze-dried CNC and CNF were added into 10 mL of solvent (water, DMF, ethanol, acetone, and chloroform), and then sonicated in an ice bath for 2 min at 100% amplitude. Both visual appearance and microscopic images of the

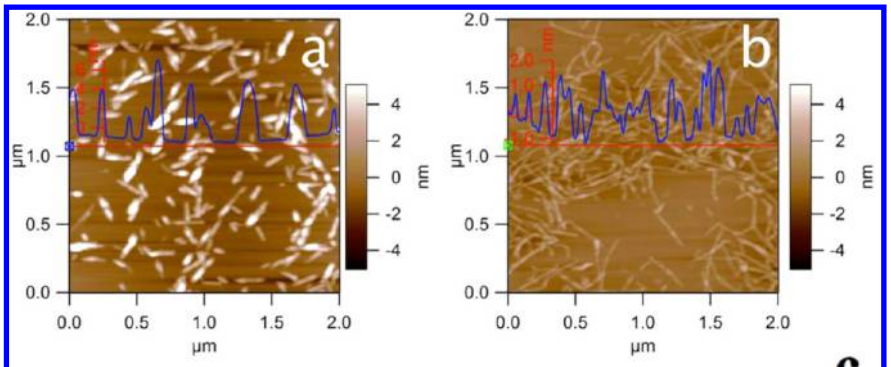

Samples	Thickness (nm)	Width (nm)	Length (nm)	Crystallite dimension (nm)	CrI (%)	Specific surface area (m^2/g)	Sulfate[a]/carboxylic[b] /carboxylates[c] content (mmol/g)
CNCs	4.7±1.3	6.4±1.2	143±31	4.2	90.7	451	0.24[a]
CNFs	1.5±0.5	2.1±0.4	up to 1 μm	2.6	63.2	1385	0.18[b], 1.11[c]

Figure 1. CNC and CNF Characteristics: AFM height images of (a) CNCs and (b) CNFs, insets are height profiles along the red lines; (c) dimensions, crystallinity and specific surface and surface charge content.

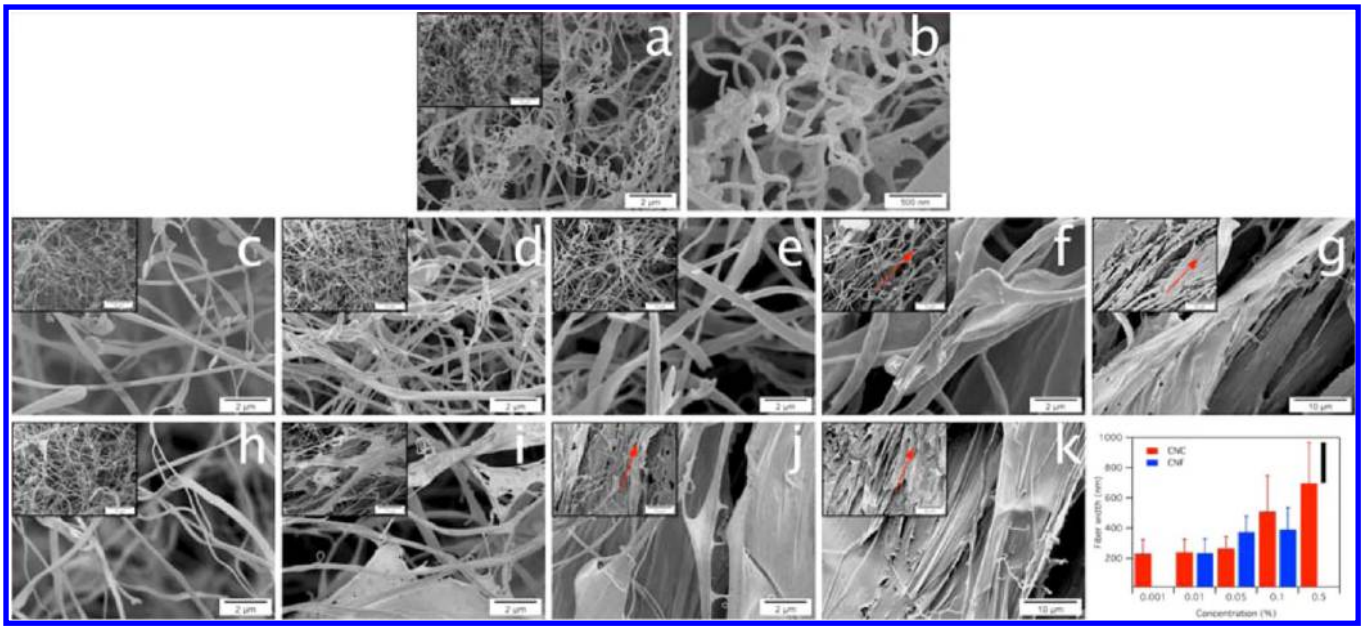

Figure 2. Submicron fibers from freeze-drying of aqueous CNC (a-g,) and CNF (h-k) suspensions (freezing at −196 °C) at various concentrations: (a,b) 0.001%, (c) 0.01%, (d) 0.05%, (e) 0.1%, (f) 0.5%, (g) 1%, (h) 0.01%, (i) 0.05%, (j) 0.1%, and (k) 0.3%. Arrows indicate the radial direction of the tube, pointing to the center. (l) Fiber diameters of freeze-dried CNCs and CNFs.

redispersed suspensions were recorded. For poorly dispersed nanocellulose/solvent systems, the suspensions were examined under a Leica DM2500 optical microscope equipped with cross-polarized filter. For well-dispersed nanocellulose/solvent systems, the suspensions were diluted to 0.0005%, dried on a freshly cleaved mica surface and observed using Asylum-Research MFP-3D atomic force microscope as previously described.

3. RESULTS AND DISCUSSION

3.1. Characteristics of CNCs and CNFs. CNCs and CNFs were derived from pure rice straw cellulose by sulfuric acid hydrolysis (64% H_2SO_4, 45 °C, 45 min)[7] and TEMPO oxidation (5 mmol/g NaClO/cellulose) coupled with blending (37 000 rpm, 30 min),[8] respectively. CNCs are rigid rodlike crystallites with average thickness (T), width (W), and length (L) of 4.7 ± 1.3, 6.4 ± 1.2, 143 ± 31 nm, respectively, and ∼20 L/W or 30 L/T aspect ratio (Figure 1a, T from AFM, W and L from TEM not shown). Both thickness (4.7 nm) and length (154 nm) of rice straw CNCs are very close to those from softwood pulp (T = 4.8 nm, L = 154 nm),[47,48] hardwood pulp (T = 4.8 nm, L = 147 nm),[3] and cotton fibers (T = 5.2 nm, L = 170 nm).[49] CNFs, on the other hand, are much finer (T = 1.5 ± 0.5 nm, W = 2.1 ± 0.4 nm) and longer (approaching 1 μm) (Figure 1b) than the 3−5 nm widths reported for wood pulp CNFs from similar TEMPO oxidation and mechanical defibrillation processes.[5,50,51] The much thinner rice straw CNFs at concentrations exceeding 0.2% have shown to

assembled into superasbrobent aerogels with unprecedented absorbency.[52] While CNCs are three times larger in both thickness and width and 1 order of magnitude lower in aspect ratio than CNFs, both CNCs and CNFs are slightly asymmetric in their cross-sectional dimensions, that is, widths being ~35% and 38% greater than thickness, respectively. Proportional to their lateral dimensions, the calculated specific surface for CNFs (1385 m^2/g) is just over three times of that for CNCs (451 m^2/g) (Figure 1c).

Sulfuric acid hydrolysis and TEMPO oxidation not only lead to individualized nanocellulose but also derivatize surface hydroxyls to sulfates and carboxyls, respectively.[53,54] The surface charge density quantified by conductometric titration was 0.24 mmol sulfate groups per g of CNC (0.04 sulfate/AG), whereas CNFs carry 0.18 mmol carboxylic (COOH) and 1.11 mmol carboxylates (COO^-Na^+) per g of CNF (0.03 COOH/AG and 0.18 COO^-Na^+/AG) (Table 1c and Figure S1 in Supporting Information).[8,55] Both CNCs and CNFs retained the expected native cellulose Iβ crystalline structure, evident by the 2θ peaks at 14.7, 16.8 and 22.7° (Figure S2 in Supporting Information) for the $1\bar{1}0$, 110, and 200 monoclinic crystallographic planes, respectively.[47] However, CNCs had a more highly crystalline structure (90.7% CrI) and larger crystallite dimension (4.2 nm) than CNFs (63.2% CrI, 2.6 nm), consistent with less reacted surfaces indicated by the lower extent of sulfation. The high CrI of rice straw CNCs is similar to CNCs from cotton (90.5%,[56] and 88.6%[49]) and *Syngonanthus nitens* (91%),[57] but much higher than those from bacterial cellulose (76.6%),[58] bleached wood pulp (66.4%),[35] rice husk (59%),[59] and pseudostems of banana plant (74%),[60] showing the crystallinity of CNCs to be highly sources dependent. The 63.2% CrI of rice straw CNFs is higher than kraft pulp CNFs (52.4%),[61] but lower than those from cotton linter (86%) and ramie (92%),[62] also showing sources dependent characteristic. With nearly one tenths of the cross-sectional area and more than 1 order of magnitude higher aspect ratio, the less crystalline CNFs appeared flexible with bends as observed by AFM.

3.2. Freezing Induced Self-Assembling of Aqueous CNC and CNF Suspensions. Rapidly freezing (−196 °C, 10 min) and lyophilization (−50 °C, 0.05 mbar, 2 days) of aqueous CNC and CNF suspensions at 0.001−1 and 0.01−0.3% respective concentration ranges produced white fluffy fibrous mass in all cases. Upon close examination by SEM, distinctly different morphologies were apparent and appeared to be both concentration and nanocellulose characteristics dependent (Figure 2). Fibers from the extremely low 0.001% CNC suspension were in bimodally distributed nanoscale (58 ± 14 nm) and submicron (218 ± 94 nm) widths (Figure 2a, b, and l). The nanofibers appear curly while the submicron fibers are straight. From 1 order of magnitude higher CNC concentrations of 0.01% and 0.05%, only submicron wide fibers with 242 ± 85 and 269 ± 76 nm average widths, respectively, were observed (Figure 2c,d and l). At yet another order of magnitude higher CNC concentrations of 0.1% and 0.5%, fibers produced were even wider at 511 ± 238 and 699 ± 270 nm, respectively, while heterogeneous ribbon-like structures were also observed (Figure 2e, f, and l), the latter eventually evolved into tens of micrometer wide film-like structures at 1% CNC concentration (Figure 2g). Thus, aqueous CNCs assembled into mostly submicron (200 to 700 nm) wide fibers with ca. 60 nm wide nanofibers observed only from 0.001% and micrometer wide films at 1%. It should be noted that CNCs readily self-assemble upon freezing and freeze-drying even at extremely dilute concentration of 0.001%, confirming SEM observation of dried individual nanocellulose to be impractical. Therefore, the dimensions and morphologies of isolated nanocellulose can only be discerned by AFM and TEM

Fibers assembled from aqueous suspensions of the much thinner and highly surface carboxylated CNFs showed similar increasing fiber widths with increasing concentrations (Figure 2h−k, l). However, the fibers assembled from aqueous CNFs and CNCs at the same concentration were distinctly different. Most homogeneous fibers with 236 ± 95 nm average width were assembled from 0.01% CNFs (Figure 2h and l), essentially the same as the 242 ± 85 nm wide fibers assembled from CNCs at the same concentration, but appearing more flexible and curly, likely due to the lower crystallinity and more than 1 order of magnitude higher aspect ratio of CNFs. As CNF concentration increased to 0.05%, a mixture of 375 ± 105 nm wide fibers and thin films (several microns wide) appeared (Figure 2i and l), dramatically different from the homogeneous 269 ± 76 nm wide fibers from CNC at the same concentration (Figure 2d). Wider (tens of microns wide) and thicker films were assembled from 0.1% CNF in the presence of traces of 393 ± 144 nm wide fibers (Figure 2j and l), while hundreds of microns wide films were observed at 0.3% CNF (Figure 2k). Massive film formation at the much lower 0.1% CNF as compared to that at 1% CNC indicates stronger association among CNFs than CNCs at similar concentrations, which is also manifested by the more viscose CNF suspension as compared to the water-like suspension of CNCs at the same 0.3% concentration. Therefore, aqueous CNFs assembled into submicron wide fibers only at low concentration of 0.01%, beginning to evolve into film-like structure at and above 0.05%. Albeit distinctly different laterally assembled CNCs and CNFs at varying concentrations, both assembled into several tens of micrometers long fibrils, indicating massive longitudinal assembling of both submicron long nanocellulose.

The critical concentrations where ribbons and films were observed occurred at 0.1−0.5% for CNCs and 0.01−0.05% for CNFs, respectively, showing massive assembling occurred at 1 order of magnitude lower concentration for the thinner but longer CNFs than rod-like CNCs. While both CNC and CNF surfaces are negatively charged, CNCs carry far less (0.24 mmol/g) charged sulfate groups that are randomly distributed on surface C2, C3 and C6 than combined carboxylate/carboxylic (1.29 mmol/g), all on surface C6. Although most CNF surface carboxylate/carboxylic was charged, i.e., 1.11 mmol/g or 86% COO^-Na^+, the carboxylate could participate in hydrogen bonding as hydrogen bond acceptor in addition to the hydrogen bonding capability of the remaining C6 carboxylic and C2 and C3 hydroxyls, all regularly spaced on the surfaces. The more readily assembled structures from CNFs are attributed to their greater ability to entangle and stronger inter-CNF hydrogen bonding capacity. At above these fiber-to-film concentrations, that is, 0.5−1% for CNCs and 0.1−0.3% for CNFs, the assembled fibers or films showed preferential alignment along the radial direction of the tube or the temperature gradient (along the red arrows in Figure 2f, g, j, and k, insets), confirming ice crystal growth or the ice templating effect.

The effect of freezing temperature on the assembled morphologies was examined by freezing CNCs (0.05%) and CNFs (0.01%) at −20 °C for 6 h and then freeze-dried, both at

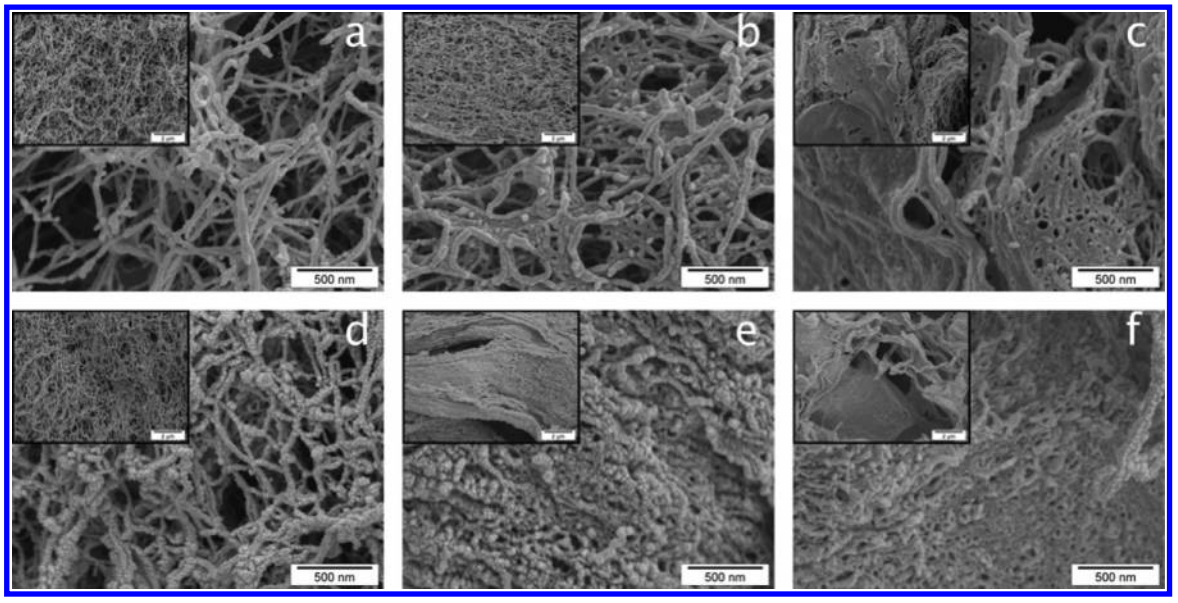

Figure 3. Nanofibers assembled from freezing (−196 °C) and freeze-drying of CNC (a−c) and CNF (d−f) in 10/90 *tert*-butanol/water suspensions at various concentrations: (a) 0.05%, (b) 0.1%, (c) 0.5%, (d) 0.01%, (e) 0.05%, and (f) 0.1%.

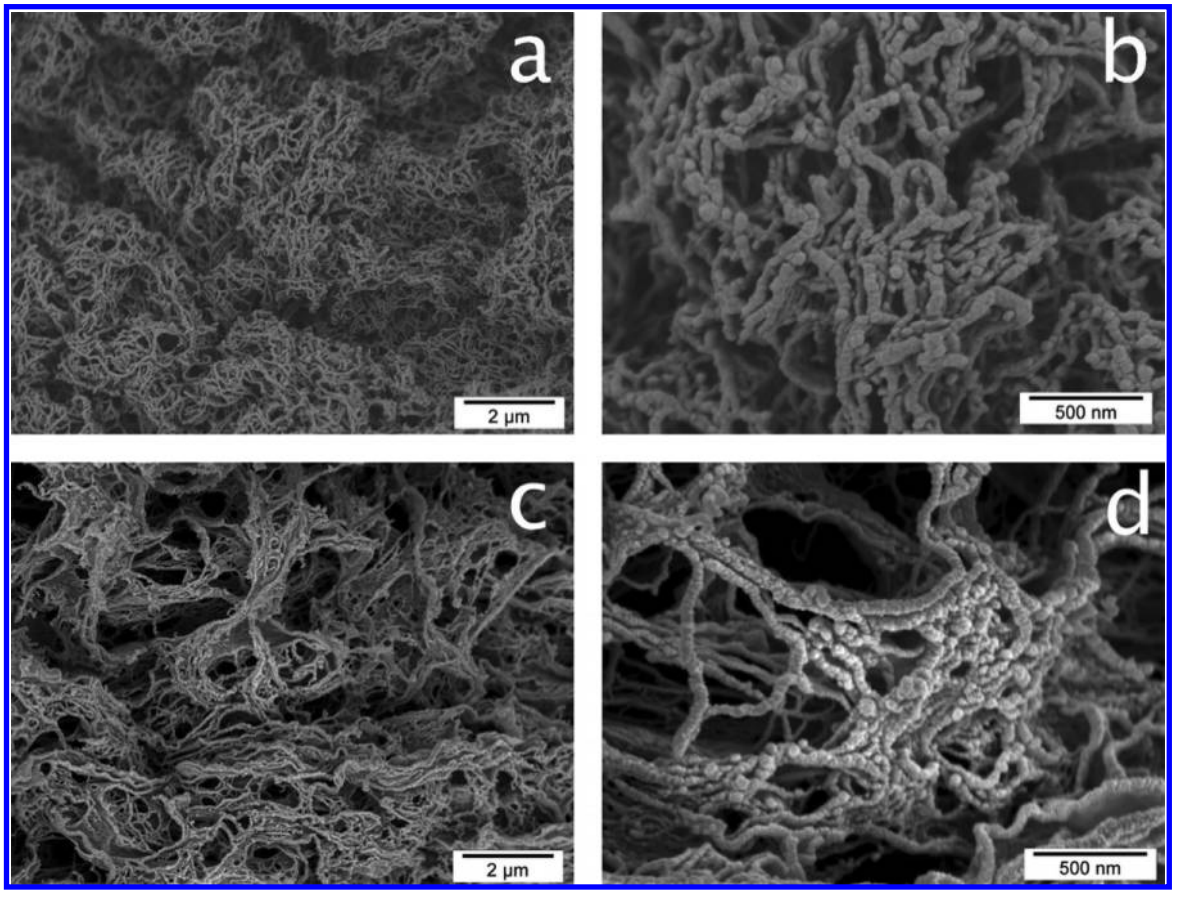

Figure 4. Nanofibers assembled from freezing (−196 °C) and freeze-drying of (a, b) 0.1% CNC in 93/7 *tert*-butanol/water and (c, d) 0.1% CNF in 50/50 *tert*-butanol/water.

concentrations below their respective critical fiber-to-film transformation concentrations. Freezing at −20 °C produced more packed solid mass, appearing as isolated films of over hundreds of microns wide under SEM (Figure S3 in Supporting Information). This is in contrast to rapid freezing at −196 °C that led to white and fluffy fibrous mass of continuous submicron wide fibers (269 ± 76 nm for CNCs in Figure 2d and 236 ± 95 nm for CNFs in Figure 2h).

In freezing aqueous nanocellulose suspensions, ice nucleation of the massive water and ice crystal propagation concentrate nanocellulose between ice crystals into close proximities, which bring about self-assembling that is further reinforced by

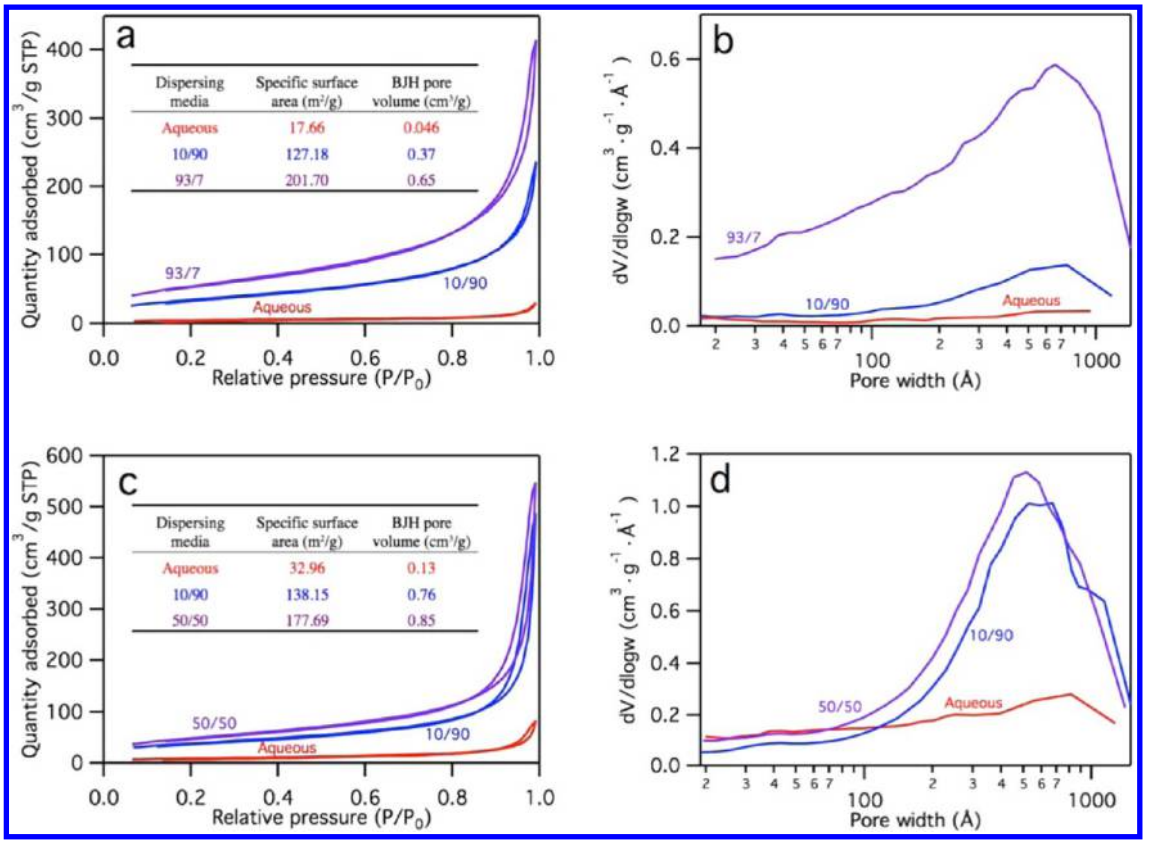

Figure 5. N_2 adsorption−desorption isotherms (a, c) and pore size distribution (b, d) of cellulose fibrous materials assembled from CNCs (a, b) and CNFs (c, d) in aqueous (red) and *tert*-butanol/water (blue and purple, with ratios marked in Figures) suspensions. Insets in a and c: specific surface areas and BJH pore volume.

extensive hydrogen bond formation upon the evaporation of surface bound water during lyophilization. Rapid freezing at −196 °C induces fast nucleation and formation of smaller ice crystals, segregating nanocellulose in numerous narrow spaces among many small ice crystals to form well separated thin fibers. In contrast, slower freezing at −20 °C induces ice nuclei growth into larger ice crystals, concentrating more nanocellulose in fewer spaces among large ice crystals to assemble into fewer but far larger aggregates or solids. Freezing temperature effects on the assembled morphologies are primarily due to ice crystal nucleation and growth rates. The fact that more concentrated nanocellulose led to increased size of assembled structures is also consistent with the increased local concentration of nanocellulose between ice crystals.

3.3. Freezing Induced Self-Assembly of CNCs and CNFs in *tert*-Butanol. The effect of *tert*-butanol on self-assembling of nanocellulose was first studied by freezing CNC and CNF dispersions in 10/90 *tert*-butanol/water at −196 °C then freeze-dried (Figure 3). The nanofibers assembled from 0.05% CNC, 0.1% CNC, and 0.01% CNF in 10/90 *tert*-butanol/water were averagely 34.3 ± 7.2 nm, 40.2 ± 6.2, and 33.0 ± 7.1 nm wide, respectively (Figure 3a, b and d), significantly smaller than 269, 511, and 236 nm widths of those assembled from aqueous counterparts (Figure 2 d, e, and h). By merely replacing 10% water with *tert*-butanol, the assembled fibers were approximately 1 order of magnitude narrower at the same nanocellulose concentrations. Most distinctively, these nanofibers were only a few micrometers in length with many free ends, indistinctly contrast to the over several tens of micrometers long fibers assembled from aqueous suspensions, manifesting great impediment of *tert*-butanol to nanocellulose associations in both lateral and longitudinal directions. This inhibitive effect could be ascribed to the different hydrogen bonding capacity between *tert*-butanol and water with nanocellulose and the steric hindrance of *tert*-butanol bound nanocellulose surfaces. Each *tert*-butanol molecule could hydrogen bond to only one nanocellulose surface hydroxyl or carboxyl, preventing it from further hydrogen bonding or polar interaction while the three bulky methyl groups add steric hindrance to limit internanocellulose association. Assembled films could be observed at similar concentrations of above 0.1% and 0.01% for CNCs and CNFs, respectively (Figure 3c, e, and f), indicating the critical concentrations for fiber-to-film transformation were unaffected by 10% *tert*-butanol. However, numerous tens of nanometer wide pores were observed on these assembled films rather than the intact smooth films from aqueous media. The appearance of these meso-pores may be explained by the formation of smaller crystals because of the added *tert*-butanol. Addition of 3−19 wt % *tert*-butanol has shown to induce crystallization of water into smaller needle-shaped ice crystals in contrast to the larger hexagonal ice crystals from pure water.[63,64]

Tert-butanol concentration was further increased to 93/7 and 50/50 *tert*-butanol/water for 0.1% CNCs and CNFs, respectively. The CNCs assembled from 93/7 *tert*-butanol/water were relatively homogeneous nanofibers with essentially identical width (40.9 ± 6.5 nm) as those from 10/90 *tert*-butanol/water (40.2 ± 6.2 nm), but even shorter with many more free ends (Figure 4a and b vs Figure 3b), indicating the longitudinal assembly of CNCs were further inhibited by

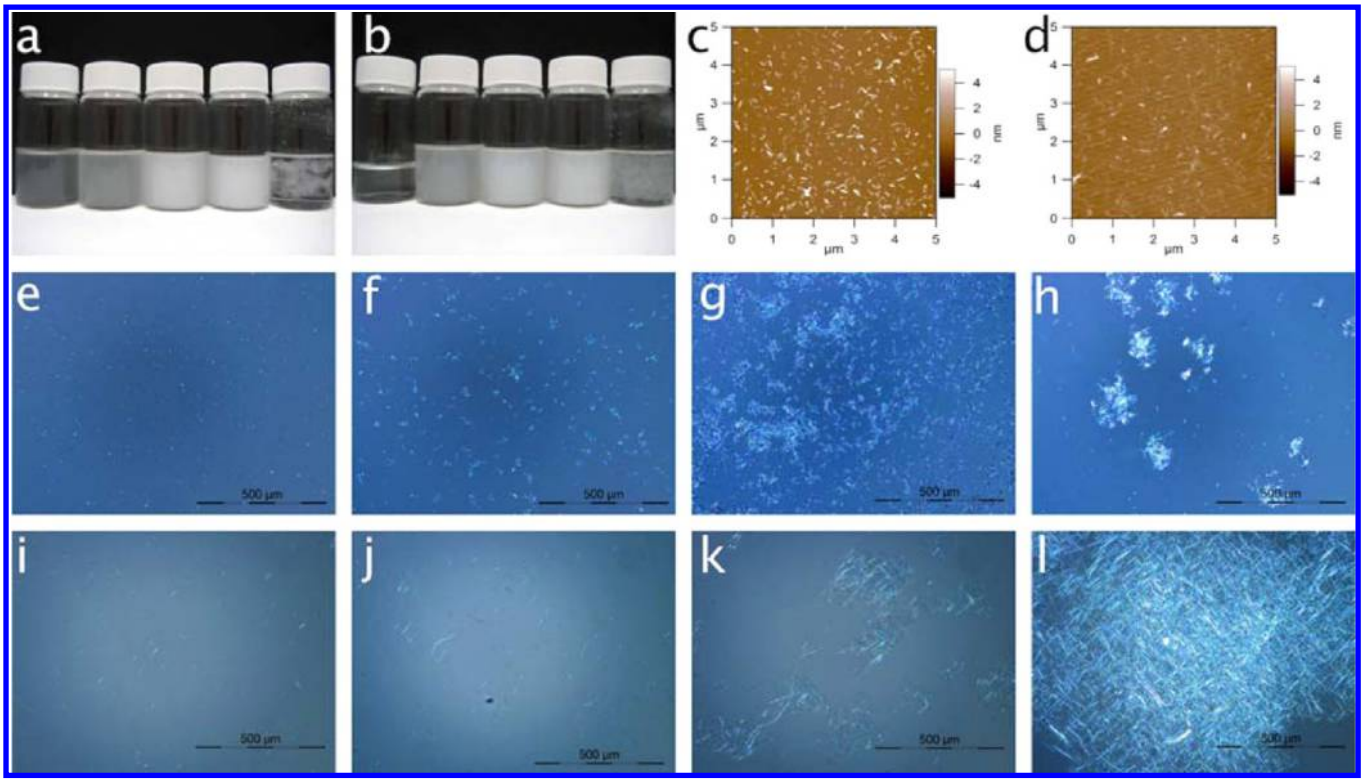

Figure 6. Redispersibility of CNC and CNF freeze-dried from 0.1% aqueous suspensions: (a) CNCs, (b) CNFs dispersed in water, DMF, ethanol, acetone, and chloroform (from left to right); AFM images of (c) CNCs and (d) CNFs dispersed in water; optical microscope images of CNCs (e–h) and CNF (i–l) dispersed in DMF (e, i), ethanol (f, j), acetone (g, k), and chloroform (h, l) under cross-polarizer.

increasing *tert*-butanol content, but not lateral assembly. For CNFs, homogeneous suspensions could be maintained in mixtures with only up to 50% *tert*-butanol, then gelled in 70/30 *tert*-butanol/water, showing highly entangled fibrillated network (Figures S4 and S5 in Supporting Information). The assembled structure from CNFs in 50/50 *tert*-butanol/water showed individual nanofibers with 42.5 ± 6.6 nm average width (Figure 4c and d), similar to those from 10/90 *tert*-butanol/water (33.0 ± 7.1 nm), as well as some aggregated nanofibers. The clearly nanofibrillar structure is in significant contrast to the extensively packed porous films from 10/90 *tert*-butanol/water (Figure 3f), clearly indicating higher *tert*-butanol concentration inhibit lateral assembly of CNFs at 0.1% concentration. Nanofibers assembled CNF in 50/50 *tert*-butanol/water were much longer than those assembled from CNCs in 93/7 *tert*-butanol/water at the same 0.1% concentration.

In conclusion, freezing induced self-assembling of both CNCs and CNFs was significantly inhibited, both laterally and longitudinally, with 10% *tert*-butanol codispersant, generating homogeneous nanofibers that are 1 order of magnitude narrower and shorter than those from 100% aqueous media. A much higher 93% *tert*-butanol did not further impact lateral assembling, but reduced the lengths of the assembled nanofibers from CNCs. Both individualized and aggregated nanofibers were assembled from CNFs at higher 50% *tert*-butanol, showing significant inhibition of CNF self-assembling in the lateral directions at 0.1% concentration as well as increased critical fiber-to-film transformation concentration with more *tert*-butanol.

3.4. Specific Surface and Pore Structure. The assembled CNCs and CNFs from 0.1% aqueous suspensions showed nearly reversible adsorption and desorption loops, typical of type II isotherms for nonporous or macroporous structures (Figure 5a and c), with 17.66 and 32.96 m^2/g BET specific surface and 0.046 and 0.13 cm^3/g cumulative pore volumes, respectively (insets, Figure 5a and c). The pore distributions showed no evidence of micropores in either case and very little meso-pores in the CNF case (Figure 5b and d). All these indicate the structures assembled from aqueous CNCs and CNFs suspensions are tightly associated with no evidence of their original nanoscale identity. From the specific surface values and assumed cylindrical shaped fibers, the calculated diameters would be 140 and 80 nm for self-assembled CNCs and CNFs, respectively, significantly smaller than the observed 511 nm wide fibers and mostly film-like appearance (Figure 2e and j). The much higher measured specific surface than gross morphology observed by SEM indicates both self-assembled structures were porous, specifically macroporous, with that from CNFs also meso-porous.

In contrast, self-assembled CNCs and CNFs from 10/90 *tert*-butanol/water suspensions absorbed significantly more nitrogen and showed type IV hysteresis isotherms (Figure 5a and c) with significantly higher 127.18 and 138.15 m^2/g BET specific surface and 0.37 and 0.76 cm^3/g cumulative pore volumes, respectively. Increasing *tert*-butanol further to respective 93/7 and 50/50 increased the specific surface further to 201.70 and 177.69 m^2/g and pore volumes to 0.65 and 0.85 cm^3/g for CNC and CNF, respectively. In all cases, pore volume in the assembled structures increased with increasing *tert*-butanol and both mesopores and macropores in the 10–100 nm range were prevalent (Figure 5b and d). Increases in both BET specific surface area and pore volume in the presence of *tert*-butanol agreed well with the reduced fiber dimensions as observed from

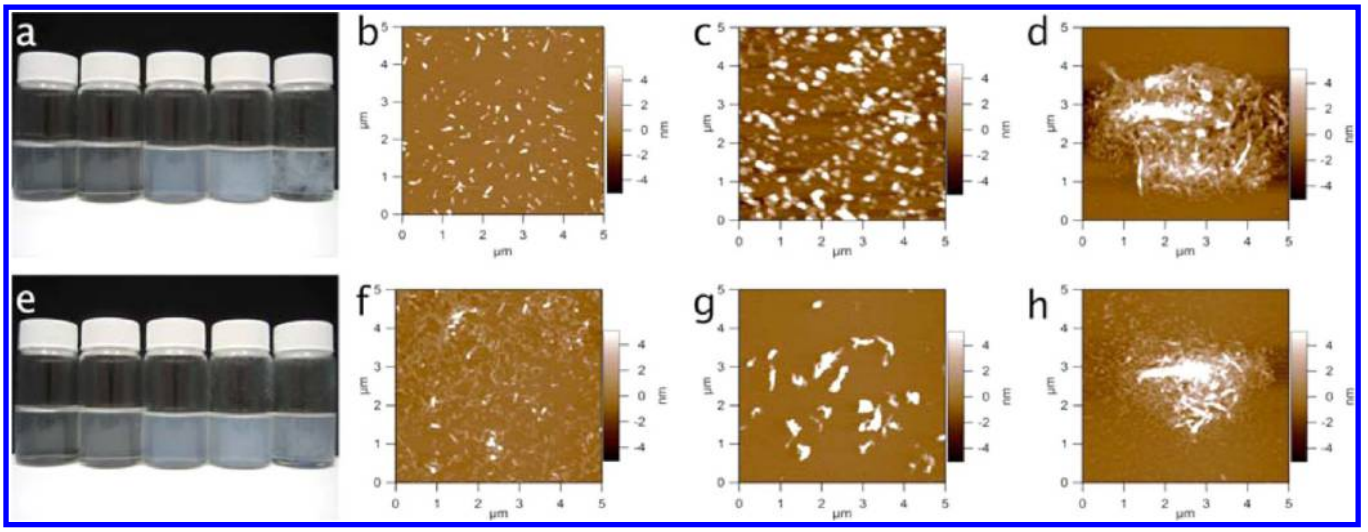

Figure 7. Redispersibility of CNC and CNF freeze-dried from 0.1% 93/7 and 50/50 *tert*-butanol/water suspension, respectively. Photograph of CNC (a) and CNF (e) dispersed (from left to right, the solvents are water, DMF, ethanol, acetone, and chloroform). AFM images of CNC (b–d) and CNF (f–h) dispersed in water (b, f), DMF (c, g), and ethanol (d, h).

SEM. The pore size distributions peaked at 74 and 67 nm for CNCs and CNFs assembled from 10/90 *tert*-butanol/water suspensions, respectively, then lowered slightly to 66 and 52 nm pores with further increases in *tert*-butanol contents.

3.5. Redispersibility of Assembled CNCs and CNFs in Various Solvents. The fibrous mass assembled from freezing (−196 °C) and freeze-drying of 0.1% CNC and CNF aqueous suspensions was redispersed in water, DMF, ethanol, acetone, and chloroform at 1 mg/mL concentration with 2 min ultrasonication. Both assembled CNCs and CNFs were readily redispersed in water to transparent suspensions (Figure 6a and b). AFM images of the redispersed CNCs and CNFs showed them to be individually separated with 3.8 ± 1.5 and 2.0 ± 0.7 nm average thickness, respectively, approximately 20% lower and 33% higher than their respective original dimensions, that is, CNCs (4.7 ± 1.3 nm) and CNFs (1.5 ± 0.5 nm). These thickness differences are not statistically significant, but the redispersed CNFs were much shorter, indicating cleavage in length possibly by ultrasonication.

The CNCs and CNFs assembled from water could not be redispersed back into nanocellulose in DMF, ethanol, acetone, and chloroform with 2 min ultrasonication. Observation by optical microscope equipped with cross-polarizers showed large micrometer sized fibers for both in DMF (Figure 6e and i) and even larger and more aggregated fibers in ethanol, acetone and chloroform, all with lower dielectric constants (Figure 6f–h and j–l). In all cases, the redispersed fibers appeared longer for those assembled from CNFs than CNCs, indicating much strongly associated CNFs from freezing and freeze-drying. Furthermore, the predominantly carboxylated CNF surfaces, that is, 1.11 mmol carboxylates per gram of CNCs, may be too highly ionized to be homogeneous dispersed in DMF. Even though lyophilized CNCs could be redispersed in DMF after extended ultrasonication (72 h),[40] it is clear that neither the fibrous mass assembled from aqueous CNCs or CNFs could be redispersed in DMF with the brief 2-min ultrasonication.

CNCs and CNFs assembled from 0.1% 93/7 and 50/50 *tert*-butanol/water suspensions, respectively, also redispersed in water well to transparent suspensions, showing isolated CNCs and CNFs with average height of 4.7 ± 1.8 and 2.2 ± 1.2 nm, respectively (Figure 7a, b, e, f), similar to those redispersed from fibers assembled from aqueous suspensions. Both CNCs and CNFs assembled from *tert*-butanol/water mixtures could also be redispersed in DMF into transparent dispersions, a significantly improvement in contrast to those assembled from aqueous suspensions. The particulates redispersed in DMF were averaged 6.0 ± 3.3 and 9.6 ± 3.3 nm thick (Figure 7a, c, e, g), 1.3 and 6.4 times of their respective original CNC and CNF thickness (Figure 1), indicating some hydrogen bonding within nanocellulose was too strong to be completely disrupted by the 2 min ultrasonication in DMF. Again, dispersions in the low dielectric constant ethanol and acetone were cloudy with larger agglomerates (Figure 7a, d, e, h and Figure S6 in Supporting Information); however, appeared light blue translucent, in contrast to the white opaque dispersions for those assembled from aqueous media, indicating better dispersion. Neither CNCs nor CNFs assembled from *tert*-butanol/water mixtures could be dispersed in chloroform (Figure S6 in Supporting Information).

In essence, the assembled structures from aqueous 0.1% CNC and CNF suspensions could be completely redispersed in water to essentially their original dimensions, showing it is possible to rapidly freeze and freeze-dry aqueous nanocellulose for storage and transportation, then redisperse into aqueous suspensions without changing their nanoscale characteristics. However, neither assembled structures from aqueous suspensions could be redispersed in any of the less polar solvents. Nanofibers assembled from CNCs and CNFs from respective 93/7 and 50/50 *tert*-butanol/water suspensions are not only much finer, but also could be redispersed in DMF with 2 min ultrasonication, a significant new property in contrast to those from aqueous suspension, but not in ethanol, acetone, or chloroform.

4. CONCLUSION

Rapid freezing (−196 °C, 10 min) and slow freeze-drying (−50 °C, 0.05 mbar, 2 days) induced self-assembling of rice straw nanocellulose, that is, 4.7 ± 1.3 nm thick, 6.4 ± 1.2 nm wide, 143 ± 31 nm long CNCs and 1.5 ± 0.5 nm thick, 2.1 ± 0.4 nm wide and up to 1 μm long CNFs, into mostly submicron (200–700 nm) wide and several tens of micrometers long fibrils, showing massive lateral and longitudinal assembling of both

nanocellulose. At the same 0.01% concentration, both CNC and CNF assembled into homogeneous fibers of similar widths, that is, 242 ± 85 for CNCs and 236 ± 95 nm for CNFs. The assembled fiber widths increased with increasing nanocellulose concentrations, then transmitted into ribbon and film like structures at 0.1−0.5% for CNCs and 0.01−0.05% for CNFs, respectively, showing stronger association among CNFs than CNCs. The extensively assembled structure from 0.1% concentration were macroporous with BET specific surface area of 17.66 and 32.96 m^2/g and cumulative pore volumes of 0.046 and 0.13 cm^3/g for CNCs and CNFs, respectively.

Same freezing and freeze-drying of 0.1% CNCs and CNFs in 10/90 *tert*-butanol/water suspension induced both nanocellulose to self-assemble into 33−40 nm wide and a few micrometers long nanofibers, approximately 1 order of magnitude smaller than those from aqueous suspensions in both widths and lengths and significantly increased specific surface and pore volume for CNCs (127.18 and 0.37 cm^3/g) and CNFs (138.15 m^2/g and 0.76 cm^3/g), indicating inhibitory effect of *tert*-butanol on nanocellulose self-assembling in both lateral and longitudinal directions. Further increased *tert*-butanol content in the media reduced longitudinal assembling of CNCs to much shorter nanofibers and reduced lateral CNF assembly at a higher concentration, both with further improved specific surface and pore volume (201.70 and 0.65 cm^3/g for CNCs and 177.69 and 0.85 cm^3/g for CNFs). While the submicron fibers assembled from aqueous suspension could only be redispersed in water, the significantly inhibited nanocellulose assembled from *tert*-butanol/water mixtures could be facilely dispersed in water and DMF with brief 2 min ultrasonication.

■ ASSOCIATED CONTENT

Supporting Information

Conductometric titration measurement for carboxylic and carboxylates on CNFs; X-ray diffractograms of CNC and CNF; Macroscopic films from freeze-drying of aqueous CNC and CNF freezing at −20 °C; SEM images and N_2 adsorption−desorption isotherms and pore distribution of nanofibers assembled from freezing (−196 °C) and freeze-drying 0.1% CNF in 70/30 *tert*-butanol/water; optical microscope images of redispersibility of CNC and CNF freeze-dried from 0.1% 93/7 and 50/50 *tert*-butanol/water suspension in acetone and chloroform. This material is available free of charge via the Internet at http://pubs.acs.org.

■ AUTHOR INFORMATION

Corresponding Author

*Tel. +1 530 752 0843. Fax: +1 530 752 7584. E-mail: ylhsieh@ucdavis.edu.

Notes

The authors declare no competing financial interest.

■ ACKNOWLEDGMENTS

Financial support for this research from the California Rice Research Board (Project RU-9) is greatly appreciated.

■ REFERENCES

(1) Jarvis, M. *Nature* **2003**, *426*, 611−612.
(2) Habibi, Y.; Lucia, L. A.; Rojas, O. J. *Chem. Rev.* **2010**, *110*, 3479−3500.
(3) Beck-Candanedo, S.; Roman, M.; Gray, D. G. *Biomacromolecules* **2005**, *6*, 1048−1054.
(4) Kose, R.; Mitani, I.; Kasai, W.; Kondo, T. *Biomacromolecules* **2011**, *12*, 716−720.
(5) Saito, T.; Nishiyama, Y.; Putaux, J. L.; Vignon, M.; Isogai, A. *Biomacromolecules* **2006**, *7*, 1687−1691.
(6) Paakko, M.; Ankerfors, M.; Kosonen, H.; Nykanen, A.; Ahola, S.; Osterberg, M.; Ruokolainen, J.; Laine, J.; Larsson, P. T.; Ikkala, O.; Lindstrom, T. *Biomacromolecules* **2007**, *8*, 1934−1941.
(7) Jiang, F.; Hsieh, Y.-L. *Carbohydr. Polym.* **2013**, *95*, 32−40.
(8) Jiang, F.; Han, S.; Hsieh, Y.-L. *RSC Adv.* **2013**, *3*, 12366−12375.
(9) Saito, T.; Uematsu, T.; Kimura, S.; Enomae, T.; Isogai, A. *Soft Matter* **2011**, *7*, 8804−8809.
(10) Iwamoto, S.; Kai, W. H.; Isogai, A.; Iwata, T. *Biomacromolecules* **2009**, *10*, 2571−2576.
(11) Saito, T.; Kuramae, R.; Wohlert, J.; Berglund, L. A.; Isogai, A. *Biomacromolecules* **2013**, *14*, 248−253.
(12) Nishino, T.; Matsuda, I.; Hirao, K. *Macromolecules* **2004**, *37*, 7683−7687.
(13) Habibi, Y. *Chem. Soc. Rev.* **2014**, *43*, 1519−1542.
(14) Lin, N.; Huang, J.; Dufresne, A. *Nanoscale* **2012**, *4*, 3274−3294.
(15) Eichhorn, S. J. *Soft Matter* **2011**, *7*, 303−315.
(16) Klemm, D.; Kramer, F.; Moritz, S.; Lindstrom, T.; Ankerfors, M.; Gray, D.; Dorris, A. *Angew. Chem., Int. Ed.* **2011**, *50*, 5438−5466.
(17) Moon, R. J.; Martini, A.; Nairn, J.; Simonsen, J.; Youngblood, J. *Chem. Soc. Rev.* **2011**, *40*, 3941−3994.
(18) Isogai, A.; Saito, T.; Fukuzumi, H. *Nanoscale* **2011**, *3*, 71−85.
(19) Saito, T.; Isogai, A. *Biomacromolecules* **2004**, *5*, 1983−1989.
(20) Wang, M. S.; Jiang, F.; Hsieh, Y.-L.; Nitin, N. *J. Mater. Chem. B* **2014**, *2*, 6226−6235.
(21) Jiang, F.; Hsieh, Y.-L. *Biomacromolecules* **2014**, *13*, 3608−3616.
(22) Sehaqui, H.; Mushi, N. E.; Morimune, S.; Salajkova, M.; Nishino, T.; Berglund, L. A. *ACS Appl. Mater. Interfaces* **2012**, *4*, 1043−1049.
(23) Huang, J.; Zhu, H. L.; Chen, Y. C.; Preston, C.; Rohrbach, K.; Cumings, J.; Hu, L. B. *ACS Nano* **2013**, *7*, 2106−2113.
(24) Sehaqui, H.; Zhou, Q.; Berglund, L. A. *Compos. Sci. Technol.* **2011**, *71*, 1593−1599.
(25) Sehaqui, H.; Salajkova, M.; Zhou, Q.; Berglund, L. A. *Soft Matter* **2010**, *6*, 1824−1832.
(26) Lee, J.; Deng, Y. L. *Soft Matter* **2011**, *7*, 6034−6040.
(27) Heath, L.; Thielemans, W. *Green Chem.* **2010**, *12*, 1448−1453.
(28) Peng, Y. C.; Gardner, D. J.; Han, Y. S. *Cellulose* **2012**, *19*, 91−102.
(29) Korhonen, J. T.; Hiekkataipale, P.; Malm, J.; Karppinen, M.; Ikkala, O.; Ras, R. H. A. *ACS Nano* **2011**, *5*, 1967−1974.
(30) Paakko, M.; Vapaavuori, J.; Silvennoinen, R.; Kosonen, H.; Ankerfors, M.; Lindstrom, T.; Berglund, L. A.; Ikkala, O. *Soft Matter* **2008**, *4*, 2492−2499.
(31) Chen, W. S.; Yu, H. P.; Liu, Y. X. *Carbohydr. Polym.* **2011**, *86*, 453−461.
(32) Chen, W. S.; Yu, H. P.; Li, Q.; Liu, Y. X.; Li, J. *Soft Matter* **2011**, *7*, 10360−10368.
(33) Lu, P.; Hsieh, Y. L. *Carbohydr. Polym.* **2012**, *87*, 564−573.
(34) Hsieh, Y. L. *J. Mater. Sci.* **2013**, *48*, 7837−7846.
(35) Han, J. Q.; Zhou, C. J.; Wu, Y. Q.; Liu, F. Y.; Wu, Q. L. *Biomacromolecules* **2013**, *14*, 1529−1540.
(36) Jiang, F.; Hsieh, Y.-L. *J. Mater. Chem. A* **2014**, *2*, 350−359.
(37) Viet, D.; Beck-Candanedo, S.; Gray, D. G. *Cellulose* **2007**, *14*, 109−113.
(38) Tang, L. M.; Weder, C. *ACS Appl. Mater. Interfaces* **2010**, *2*, 1073−1080.
(39) Beck, S.; Bouchard, J.; Berry, R. *Biomacromolecules* **2012**, *13*, 1486−1494.
(40) van den Berg, O.; Capadona, J. R.; Weder, C. *Biomacromolecules* **2007**, *8*, 1353−1357.
(41) Missoum, K.; Bras, J.; Belgacem, M. N. *Biomacromolecules* **2012**, *13*, 4118−4125.
(42) Capadona, J. R.; Shanmuganathan, K.; Trittschuh, S.; Seidel, S.; Rowan, S. J.; Weder, C. *Biomacromolecules* **2009**, *10*, 712−716.

(43) Samir, M.; Alloin, F.; Sanchez, J. Y.; El Kissi, N.; Dufresne, A. *Macromolecules* **2004**, *37*, 1386−1393.
(44) Okita, Y.; Fujisawa, S.; Saito, T.; Isogai, A. *Biomacromolecules* **2011**, *12*, 518−522.
(45) Brunauer, S.; Emmett, P. H.; Teller, E. *J. Am. Chem. Soc.* **1938**, *60*, 309−319.
(46) Barrett, E. P.; Joyner, L. G.; Halenda, P. P. *J. Am. Chem. Soc.* **1951**, *73*, 373−380.
(47) Jiang, F.; Esker, A. R.; Roman, M. *Langmuir* **2010**, *26*, 17919−17925.
(48) Kittle, J. D.; Wondraczek, H.; Wang, C.; Jiang, F.; Roman, M.; Heinze, T.; Esker, A. R. *Langmuir* **2012**, *28*, 11086−11094.
(49) Lin, N.; Dufresne, A. *Nanoscale* **2014**, *6*, 5384−5393.
(50) Saito, T.; Kimura, S.; Nishiyama, Y.; Isogai, A. *Biomacromolecules* **2007**, *8*, 2485−2491.
(51) Shinoda, R.; Saito, T.; Okita, Y.; Isogai, A. *Biomacromolecules* **2012**, *13*, 842−849.
(52) Jiang, F.; Hsieh, Y. L. *J. Mater. Chemistry A* **2014**, *2*, 6337−6342.
(53) Lu, P.; Hsieh, Y. L. *Carbohydr. Polym.* **2010**, *82*, 329−336.
(54) Jiang, F.; Kittle, J. D.; Tan, X. Y.; Esker, A. R.; Roman, M. *Langmuir* **2013**, *29*, 3280−3291.
(55) Jiang, F.; Dallas, J. L.; Ahb, B. K.; Hsieh, Y.-L. *Carbohydr. Polym.* **2014**, *110*, 360−366.
(56) Gu, J.; Catchmark, J. M.; Kaiser, E. Q.; Archibald, D. D. *Carbohydr. Polym.* **2013**, *92*, 1809−1816.
(57) Siqueira, G.; Abdillahi, H.; Bras, J.; Dufresne, A. *Cellulose* **2010**, *17*, 289−298.
(58) Martinez-Sanz, M.; Lopez-Rubio, A.; Lagaron, J. M. *Carbohydr. Polym.* **2011**, *85*, 228−236.
(59) Johar, N.; Ahmad, I.; Dufresne, A. *Ind. Crops Prod.* **2012**, *37*, 93−99.
(60) Mueller, S.; Weder, C.; Foster, E. J. *RSC Adv.* **2014**, *4*, 907−915.
(61) Li, Q. Q.; Renneckar, S. *Biomacromolecules* **2011**, *12*, 650−659.
(62) Saito, T.; Okita, Y.; Nge, T. T.; Sugiyama, J.; Isogai, A. *Carbohydr. Polym.* **2006**, *65*, 435−440.
(63) Kasraian, K.; Deluca, P. P. *Pharm. Res.* **1995**, *12*, 491−495.
(64) Kasraian, K.; Deluca, P. P. *Pharm. Res.* **1995**, *12*, 484−490.